Separation and Purification Technology 251 (2020) 117346

Contents lists available at ScienceDirect

Separation and Purification Technology

journal homepage: www.elsevier.com/locate/seppur

Spherical montmorillonite-supported molybdenum disulfide nanosheets as a self-sedimentary catalyst for organic pollutants removal

Hongzhen Wang[a], Ning Wang[b,d,*], Fushuai Wang[e], Fengyan Xiao[b], Dawei Pan[b,c,d,*]

[a] Qingdao University of Science and Technology, Qingdao 266001, PR China
[b] CAS Key Laboratory of Coastal Environmental Processes and Ecological Remediation, Shandong Key Laboratory of Coastal Environmental Processes, Research Center for Coastal Environmental Engineering and Technology of Shandong Province, Yantai Institute of Coastal Zone Research, Chinese Academy of Sciences, Yantai 264003, PR China
[c] University of Chinese Academy of Sciences, Beijing 100049, PR China
[d] Center for Ocean Mega-Science, Chinese Academy of Sciences, 7 Nanhai Road, Qingdao 266071, PR China
[e] Yantai University, Yantai, Shandong Province 264005, PR China

ARTICLE INFO

Keywords:
Spherical montmorillonite
MoS_2
Catalyst
Organic pollutants

ABSTRACT

Water containing organic and carcinogenic pollutants has become a serious environmental problem, threatening the life of the aquatic ecosystem and human beings. Molybdenum disulfide (MoS_2), especially monolayered MoS_2 sheets, has been proven as an effective catalyst for degradation of organic contaminants due to its more exposed edges and active sites for electron transfer. However, monolayered MoS_2 nanosheets easily aggregate due to their high surface energy and strong π-π electron interaction, heavily affecting the catalytic performances. In addition, monolayered MoS_2 nanosheets with small tiny size are difficult to recover from the mixture, restricting the capacity of recyclability and further mass application. Herein, we solved these issues via supporting the small tiny MoS_2 nanosheets on spherical montmorillonite (SMt). The SMt can not only provide large pore volume and specific surface area for supporting abundant MoS_2 but also reduce the fouling and enhance the transport during the mass production process. The prepared microspheres exhibited a high catalytic activity towards organic pollutants including methylene blue (MB) and 4-nitrophenol (4-NP) in the presence of $NaBH_4$ due to the strong adsorption capacity of SMt and the large catalytic surface area for electron transfer. Furthermore, the micro-sized granular catalyst can be facile recovered and reused without any devices involved due to the excellent self-sedimentary capacity and large size. Moreover, the catalytic performance and the morphology were almost unaltered after recycling 20 times. Our straightforward strategy to solve the issues through porous micro-sized self-sedimentary SMt supporting tiny monolayered MoS_2 nanosheet with high catalytic activity facilitates the practical application of these kinds of catalyst towards the reduction of organic and carcinogenic pollutants.

1. Introduction

Most of the organic dyes and their intermediates are carcinogenic and easily soluble in water [1]. Very low concentration in water can alter the color, thus changing the refraction index of water, which is not only caused the visual pollution but also interfered with the absorb sunlight of aquatic life [2–5]. To solve this problem, a variety of approaches have been developed to remove these pollutants, including physical adsorption [6,7], chemical and biological methods [8]. Among them, chemical catalytic method has been proved as an effective approach to fast degradation with low cost and easy operation [9–14]. Layered ultrathin two-dimensional (2D) nanomaterials have become one of the most promising catalytic materials due to their capacity of providing abundant active sites for catalysis [15,16]. As one of the typical 2D nanomaterials, molybdenum disulfide (MoS_2) nanosheets consist of covalently bonded S-Mo-S layers [17]. Compared with bulk MoS_2, mono- or few layered MoS_2 nanosheets provide abundant active sites for catalytic reduction of organic pollutants due to its under-coordinated sulfur atoms at the edges [18]. However, the nanosheets easily stack together due to van der Waals interaction during the

* Corresponding authors at: CAS Key Laboratory of Coastal Environmental Processes and Ecological Remediation, Shandong Key Laboratory of Coastal Environmental Processes, Research Center for Coastal Environmental Engineering and Technology of Shandong Province, Yantai Institute of Coastal Zone Research, Chinese Academy of Sciences, Yantai 264003, PR China.
E-mail addresses: nwang@yic.ac.cn (N. Wang), dwpan@yic.ac.cn (D. Pan).

https://doi.org/10.1016/j.seppur.2020.117346
Received 2 June 2020; Received in revised form 29 June 2020; Accepted 3 July 2020
Available online 10 July 2020
1383-5866/

catalytic process, thereby heavily decrease the number of active sites and catalytic activity. Previously, nanoparticles such as carbon nanotube [19], graphene [20,21], and TiO_2 [22] were used as the nano-supported substrate to disperse and anchor the MoS_2 nanosheets. These nano-sized substrates were well hybridized or wrapped by the MoS_2 nanosheets to obtain the stable carbon nanotube/MoS_2, graphene/MoS_2, and TiO_2/MoS_2 nanocomposites. Nevertheless, the application of these fabricated nanocomposites was still limited by the critical issues of recyclability due to their tiny nano size.

Montmorillonite (Mt) is a natural nanomaterial, has strong adsorption capacity and has been used as a good substrate for supporting MoS_2 [23–29]. For example, Peng et al. designed and successfully fabricated Mt/MoS_2 catalyst with MoS_2 nanosheets intercalating in the interlayer of Mt [30] and MoS_2 nanosheets depositing on the surface of Mt [31]. Although the prepared Mt/MoS_2 catalyst exhibited a good catalytic activity towards organic pollutant 4-nitrophenol (4-NP), their mass applications are still restricted by the problem of recyclability because the deposit rate of Mt based catalyst in the mixture is highly limited by the excellent hydrophilicity and swelling ability of Mt. Therefore, a great number of recovered devices are involved which heavily increases the cost of wastewater treatment.

Spray-drying is a proven technique in the industry to fabricate granulation with microsize to millimeter-size [32]. In our previous work, Mt were granulated to spherical micro-sized microsphere through this technology [33–35]. The stacked Mt forms a porous structure and provides abundant surface areas to support active sites. In addition, the granular treatment can obviously enhance the transport ability during the productive process, facilitating mass prodution of these kinds of catalysts [36]. Furthermore, the density of the prepared granular Mt microsphere is much higher than the mixture, which can be self-sedimentary and easy recovered from the bottom. In this work, we fabricated micro-sized spherical Mt (SMt) with large specific surface areas, followed by adhering to the tiny MoS_2 nanosheets on the surface of SMt through the polydopamine (PDA) coating [37]. PDA has been demonstrated the strong adhesion on various substrates [38]. The model organic pollutants, methylene blue (MB) and 4-nitrophenol (4-NP) were selected to evaluate the catalytic performances. Moreover, the recyclability was investigated. As we know, this is the first report of synthesized SMt/MoS_2 for catalytic reduction of MB and 4-NP, successfully solving the engineering problem through a physical method.

2. Experimental

2.1. Chemicals

All chemicals and reagents were used as received without any further purification. They include dopamine hydrochloride (DA, Sigma Aldrich, ≥ 98.0%), monolayered molybdenum disulfide (MoS_2, Sigma-Aldrich, ≥ 98.0%), montmorillonite (Mt, $(Na, K, Ca)_{0.33}(Al_{1.67}Mg_{0.33})Si_4O_{10}(OH)_2{\cdot}nH_2O$), Sinopharm Chemical Reagent Co. Ltd., China, ≥98.0%), methylene blue (MB, Tianjin Guangfu Reagent Co., China, ≥98.0%), 4-nitrophenol (4-NP, Tianjin Guangfu Reagent Co., China, ≥98.0%), sodium borohydride ($NaBH_4$, Sinopharm Chemical Reagent Co. Ltd., China, ≥99.0%), and Tris-HCl buffer (Beijing Solarbio Science & Technology Co., Ltd, China).

2.2. Granulation of Mt and fabrication of spherical Mt supported MoS_2

Spray drying technology was applied to fabricate spherical Mt (SMt). First, 10.0 g Mt was mixed with 100 mL ethanol and sonicated for 4 h. Then the suspension was adding to the spray-dryer (YC-015, Shanghai Pilotech Instrument & Equipment Co. Ltd) using a peristaltic pump. The feed rate was set as 50 mL min^{-1} and the drying temperature was set as 110 °C, respectively. Finally, the granular SMt with the mean size of about 20 μm was obtained. The prepared SMt was used as the substrate to support MoS_2. Typically, 1.0 g DA and 20 mM Tris-HCl buffer were added in 200 mL water to form the mixture. The pH was adjusted to 8.5 using 0.1 M of NaOH solution. After the color of the solution changed to dark yellow, 2.0 g SMt was added to form the suspension. Through 6 h shaking, the color of suspension changed to black and then filtered. The black product was fully washed by a 25% isopropyl alcohol-water solution and then dried in a vacuum oven at 60 °C for 24 h to obtained the black microsphere. On the other hand, the monolayered MoS_2 nanosheets were mixed in aqueous solution with a concentration of 0.1 mg·mL^{-1}, followed by ultrasound treatment for at least 4 h via a cell disruptor to get the dark black suspension. The dark black suspension was separated by the centrifugal separation at 12,000 rpm for 2 min. The faint yellow supernatant was extracted and mixed with the prepared black microsphere using a rotator for at least 6 h. After the filter separation, the microspheres were dried to obtain the final product.

2.3. Characterization

The Fourier transform infrared (FTIR) spectra of samples were obtained through a Perkin-Elmer 2000 Fourier transform infrared spectrometer with KBr pressed pellets. Scanning electron microscopy (SEM) was performed using a Jeol S4800 scanning electron microscope and an energy-dispersive detector. Transmission electron microscopy (TEM) and atomic force microscopy (AFM) were carried out using a JEM-2200 transmission electron microscope and Multi-Mode 8 atomic force microscope, respectively. X-ray diffraction (XRD) measurements were performed with Bruker D8-Advantage powder diffractometer using Cu Kα radiation (40 kV, 110 mA). X-ray photoelectron spectroscopy (XPS) measurements were taken using Thermo EscaLab 250Xi spectrometer. Nitrogen adsorption measurements were carried out at 77 K using an ASAP2020 analyzer. The UV absorption spectra were measured using a PERSEE UT 1810 UV–vis spectrometer.

2.4. Adsorption experiment

10.0 mg samples were engaged in a 100 mL aqueous solution containing 100 mg L^{-1} MB and fully mixed. Then the UV–vis absorption spectra of organic pollutants at a certain interval were recorded. The removal percentages of organic pollutants are calculated following the equation (1) [6]:

$$R = \left(\frac{C_0 - C_t}{C_0}\right) \times 100\% \quad (1)$$

Where R is the removal percentage of organic dyes, the C_o (mg L^{-1}) and C_t (mg L^{-1}) are the initial dye concentration and the concentration of reaction time, respectively.

The equilibrium concentration is calculated according to equation (2) [39]:

$$q_e = (C_0 - C_e)V/W \quad (2)$$

Where q_e is the amounts of organic pollutants adsorbed on the samples at equilibrium, C_0 (mg L^{-1}) and C_e (mg L^{-1}) are the initial and equilibrium concentrations of organic pollutants solution, respectively, V is the volume of the reaction solution (L) and W is the mass (g) of the samples.

The reduction efficiency of organic pollutants is calculated following the equation (3):

$$E = \left(\frac{C_0 - C_t}{C_0}\right) \times 100\% \quad (3)$$

Where E is the reduction efficiency of organic pollutants, the C_o (mg L^{-1}) and C_t (mg L^{-1}) are the initial and equilibrium concentration of organic pollutants, respectively.

Scheme 1. The synthesized route for the fabrication of SMt/MoS_2 microsphere, including the first spray-drying and further fixed tiny MoS_2 nanosheets on the prepared SMt through dopamine chemistry method.

2.5. Catalytic reduction

The catalytic reduction of organic dyes was carried out to assess the catalytic activity and reusability of the prepared microsphere. The calibration curves of organic dyes and their intermediates are shown in Fig. S1. Typically, 10 mL organic dyes (250 mg L^{-1}) and 20 mg (200 mg L^{-1}) catalyst were mixed with 80 mL deionized water. After fully stirring, 10 mL $NaBH_4$ (0.5 M) aqueous solutions was added. As the color of organic dyes vanished, the prepared microsphere was easily separated from the mixture due to the self-sedimentary property. Then, the catalyst was further added to the new solution containing organic dyes and $NaBH_4$ to finish one cycle. All the processes were fully recorded by the UV–vis spectrometer.

3. Results and discussion

3.1. Synthesis and characterization of SMt/MoS_2 microspheres

Porous granular Mt substrates were first prepared through the spray-drying technology. As shown in Scheme 1, after fully sonicated with ethanol, the mixed suspension was granulated through a spray dryer. The granular Mt was modified by dopamine and a black coating was formed on the surface. The strong adhesion capacity of PDA coating could easily fix the tiny MoS_2 nanosheets and thus fabricated the SMt/MoS_2 microsphere.

The granulation process of Mt is not only enhanced the size of Mt but also improved the pore size and flowability of the prepared catalyst [36]. Therefore, the morphology was observed by the SEM, TEM, and AFM. As shown in Fig. 1a, the pristine Mt exhibits an amorphous morphology with the Mt sheets loose stacking (Fig. S2a). After the spray-drying process, the granular particle with a smooth surface and a mean diameter of about 20 μm were successfully fabricated (Fig. 1b). The PDA coated process has almost unaltered the morphology (Fig. 1c). However, the obviously rough surface could be observed after deposited MoS_2 nanosheets (Fig. 1d). Difference from the prinstine Mt, a dense and porous morphology with Mt sheets tight stacking can be observed from Fig. S2b. As shown in the inset of Fig. 1d and Fig. S3, a thin ~4 nm layer was well deposited on the SMt. The small nanosheets were determined to be MoS_2, exhibiting strong Mo and S element peaks by EDX shown in Fig. S4. The crystal phases of MoS_2, SMt, and SMt/MoS_2 microsphere were analyzed by X-ray diffraction, and the data is exhibited in Fig. 2. The SMt with the crystallite size of 14.9 nm calculated from the (1 0 0) peak using Scherrer equation contained smectite (fcc, JCPDS card no. 13-0135) and quartz (fcc, JCPDS card no. 46-1045) [40]. The peaks at 2θ of 14.2°, 32.9°, 39.1°, 48.5°, and 58.3° appear, which can be assigned to the (0 0 2), (1 0 0), (1 0 3), (1 0 5), and (1 1 0) crystal faces of 2H-MoS_2 (fcc, JCPDS card no. 37-1492), confirming the successfully supported MoS_2 on the SMt (Fig. 2) [20,25]. The crystallite size of MoS_2 nanosheets was estimated from (0 0 2) peak as 7.7 nm, which is similar to the result of AFM (the thickness of the nanosheets is about 4 nm, Fig. 1e). The small-sized nanosheets can be easily supported on the micro-sized SMt substrates and provided abundant active sites for the reaction. For the SMt/MoS_2 microsphere, it exhibits the peaks of SMt and MoS_2, reflecting the good composition of SMt/MoS_2 microsphere. The crystallite size of SMt/MoS_2 microsphere was calculated as 14.5 nm, which is almost the same with the SMt, demonstrating the higher content of SMt in the SMt/MoS_2 microsphere. XPS measurements were carried out to investigate the surface elemental composition and chemical status of the prepared microsphere. As shown in Fig. 1f, the peaks corresponding to C, O, Si, S, Al, and Mo can be observed, well consistent with the formation of SMt/MoS_2 microsphere. The atomic percentages of Mo and S elements on the surface of the microsphere were calculated as 0.11% and 0.17%, which is well agreeing with the theoretical values for MoS_2. As shown in Fig. S5, for the pristine MoS_2 nanosheets, the peaks of Mo $3d_{3/2}$, Mo $3d_{5/2}$, and S 2 s are 233.1 eV, 229.7 eV, and 226.9 eV, respectively. The higher peak at 237.1 eV is assigned to the Mo $3d_{3/2}$ of MoO_3, which is derived from the adsorbed oxygen molecule [20]. For the samples of SMt/MoS_2 microsphere, no peak of MoO_3 can be observed (Inset of Fig. 1f), demonstrating the no effect of catalytic activity of SMt/MoS_2 microsphere. Furthermore, the peaks of Mo 3d are shifted to the higher energy value, reflecting the electronic interaction between MoS_2 and SMt. The enhanced interaction facilitates the improve the stability of microsphere, thereby maintaining the catalytic activities and benefiting the recovery and reuse. In addition, corresponding to the TEM image, the EDX mapping of Mo and S elements exhibit the same region, demonstrating the immobilization supporting of MoS_2 nanosheet in the fabricated microsphere (Fig. 3). Furthermore, the loading of Mo was quantified by ICP/MS to be 0.4 wt% upon dissolving SMt/MoS_2 microsphere in the strong acid, that is, the loading of MoS_2 was calculated to be 0.67 wt%. Considered the small tiny size MoS_2 uniformly dispersion on the SMt, the content of loading MoS_2 nanosheet can provide the abundant tiny active sites for catalytic reduction of organic pollutants.

3.2. Adsorption experiments

Through the granulation process, the Mt was stacked to the 2D microsphere, thus the changes of specific surface area and pore properties were measured by the N_2 adsorption. As shown in Fig. 4a and Table 1, compared with pristine Mt with a BET specific surface area of 8.2 m^2 g^{-1} and a total pore volume of 0.1 cm^{-3}/g, the values of granular SMt greatly improved to 60.6 m^2/g and 0.38 cm^{-3}/g, respectively, reflecting the well pore-making ability of spray-drying. Furthermore, the values were slightly decreased to 45.6 m^2/g and 0.24 cm^{-3}/g after the surface coating process and further decreased to 31.3 m^2/g and 0.20 cm^{-3}/g after the supporting process, which is still much higher than pristine Mt. The decreased values after the supporting process is mainly due to the weak N_2 adsorption capacity of MoS_2, as shown in Fig. 4a and Table 1. The large pore size will benefit the adsorption and catalytic reduction of organic dyes due to the opportunity for contacting with the catalyst and organic dyes. The adsorption towards organic dyes was monitored by UV–Vis absorption spectra and MB with the band of 665 nm was selected as a model here. Samples including pristine Mt, SMt, PDA-coated SMt, and SMt/MoS_2 exhibited similar adsorption with three stages, the first fast adsorption process, gradually increased stage, and the final equilibrium stage. Although all samples exhibited similar first fast adsorption behaviors, the gradual stage is quite different due to the differences of the intra-particle diffusion-rate controlling process. Compared with the pristine Mt, the intra-particle diffusion-rate of SMt, PDA-coated SMt, and SMt/MoS_2 is prolonged. The samples reach the equilibrium stage as the max

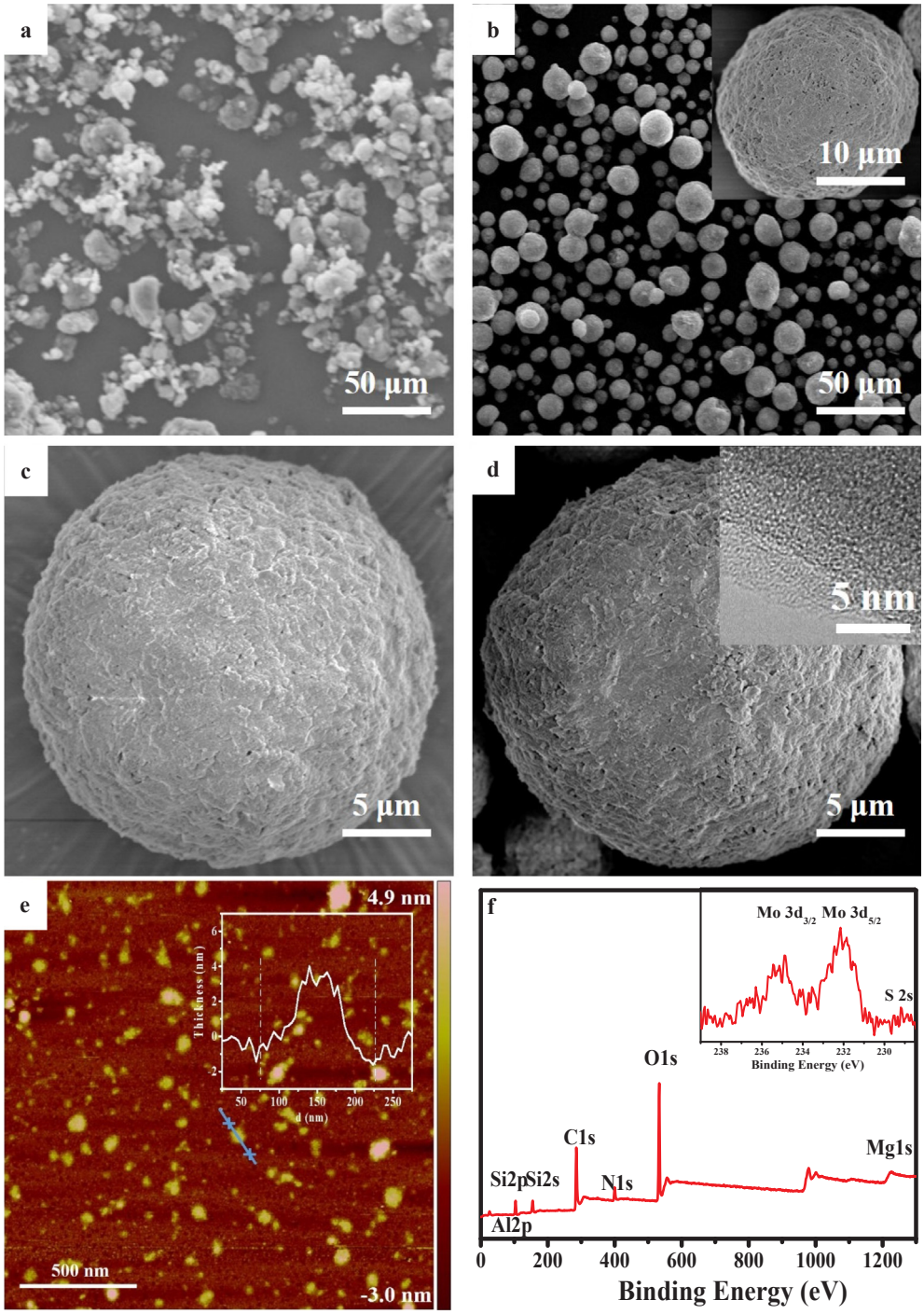

Fig. 1. SEM images of the Mt (a), SMt (b) with inset enlarging image, PDA@SMt (c) and SMt/MoS_2 (d) microspheres with inset high-resolution TEM spectra. AFM image with inset corresponding thickness of MoS_2 nanosheet (e). XPS spectra of SMt/MoS_2 with inset high-resolution XPS spectra of Mo 3d and S 2s regions (f).

adsorption is achieved (Fig. 4b). Among the samples, SMt exhibited the largest adsorption capacity of 992 mg g^{-1}, which is increased about 68.7% compared with pristine Mt. It can be attributed to the well granular process of Mt. SMt/MoS_2 slightly decreased the adsorption capacity to 870 mg g^{-1}, the value is much higher than other substrates reported in the works of literature (150 mg g^{-1} [41], 365 mg g^{-1} [22]). The enhanced adsorption ability can effectively improve the concentration of organic pollutants near the surface of the catalyst, thus improve the catalytic activity [39]. As the high adsorption capacity was obtained, the high catalytic performance is highly desirable.

3.3. Catalytic properties

The catalytic capacity of the prepared SMt/MoS_2 microsphere was evaluated through the color variation of organic dyes suffering from the catalytic reduction under $NaBH_4$. The peaks of MB and 4-NP, with the initial peak at 665 nm and 400 nm, respectively, were decreased with the prolonging catalytic reduction time. The process can be easily monitored by UV–vis spectroscopy. As shown in Fig. 5a and 5b, the absorbance peak decreases rapidly within 7 min and 6 min, respectively. The catalytic reduction process is not only eliminated the visual pollution but also alter the carcinogenicity to low and no bioactivity [34]. For example, upon the catalytic reduction process, the color of the

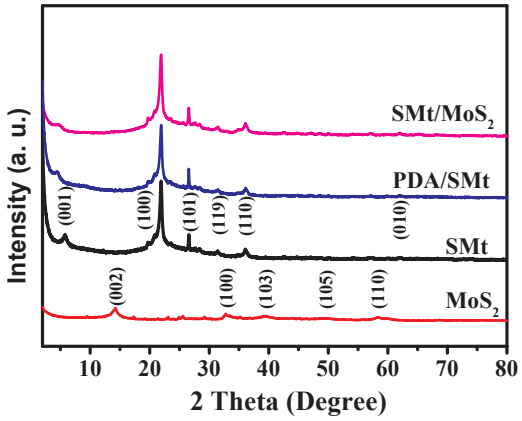

Fig. 2. XRD patterns of SMt, MoS_2, PDA/SMt, and SMt/MoS_2.

MB solution changed from blue to almost colorless, accordingly, the carcinogenic MB was altered to inactive form leucomethylene blue (LMB) [35]. Furthermore, reaction kinetics were investigated. As shown in Fig. 5c, both the catalytic processes of samples exhibit the linear relationships, demonstrating the pseudo-first-order reaction kinetics. From the linear relation of ln (C_t/C_0) with the reaction time, the apparent reduction rate constant (K) was obtained. The values of K were 0.381 min^{-1} and 0.307 min^{-1} for MB and 4-NP, respectively. The catalytic mechanism of SMt/MoS_2 microsphere is based on the electron transfer from the electron donor to the electron accepter [35]. The catalytic activity is mainly related to the surface area providing for electron transfer. Thus, the optimized K can be obtained through tailoring the concentration of catalyst. As shown in Fig. 5d, the K values can increase linearly to 0.755 min^{-1} with the concentration of SMt/MoS_2 microsphere increasing from 200 mg L^{-1} to 1000 mg L^{-1} and unaltered concentration of 4-NP and $NaBH_4$ (250 mg L^{-1} and 0.5 M, respectively). The K towards 4-NP is much higher than the MoS_2 (0.235 min^{-1}) and Mt/MoS_2 (0.874 min^{-1} and 0.723 min^{-1}) reported in the literature due to the good dispersion of MoS_2 nanosheets and high adsorption of SMt substrates towards organic dyes [30,31].

3.4. Recyclability examination

Considered the cost of MoS_2 and water containing organic pollutants, recyclability is the most promising approach for the application of the prepared SMt/MoS_2 microsphere. In this work, successive 20 cycles were applied to evaluate the recyclability of prepared catalysts. As shown in Fig. 6a and b, SMt/MoS_2 exhibits excellent catalytic stability achieving almost 100% efficiency in the 15 cycles and slightly decreasing less than 1.5% in the 20 cycles. Furthermore, as shown in Fig. 6c and d, the catalytic performance is almost unaltered upon 20 cycles. The K decreased by less than 5%. The mass loss percent of SMt/MoS_2 microsphere after recovery was weighted. After the centrifugation process, the values of the microspheres after 1, 5, 10, and 20 cycles for catalytic reduction of MB were decreased by 98.5 wt%, 97.2 wt%, 96.4 wt%, and 95.5 wt%, well agreeing with the decreased ratio of K. Thus, the slightly decreased K after recyclability experiment can be attributed to the mass loss of catalyst. Furthermore, as shown in Fig. 6e and f, the morphology of the prepared SMt/MoS_2 microsphere was almost unchanged after 20 cycles. In addition, as shown in Fig. S6, the XRD pattern of SMt/MoS_2 microsphere after catalytic cycle 20 times was almost unaltered. All their results reflect the excellent stability of the prepared microsphere.

4. Conclusions

The micro-sized granular SMt/MoS_2 microsphere was facile fabricated through the polydopamine method. MoS_2 nanosheets stably fixed on the surface of porous SMt, effectively solving the aggregation problem and further providing the abundant active sites. Besides, the prepared microsphere can effectively adsorb the organic pollutants due to its porous structure, thus, improved the concentration of organic pollutants near the surface of catalysts. These advantages validly facilitate the catalytic performance of organic pollutants. Furthermore, the prepared SMt/MoS_2 microsphere can be easily recovered from the mixture without any device involved due to the self-sedimentary property. After recycling 20 times, the morphology of SMt/MoS_2 microsphere still keep stable and the catalytic reduction efficiency was almost unaltered. Our straightforward approach to solving the

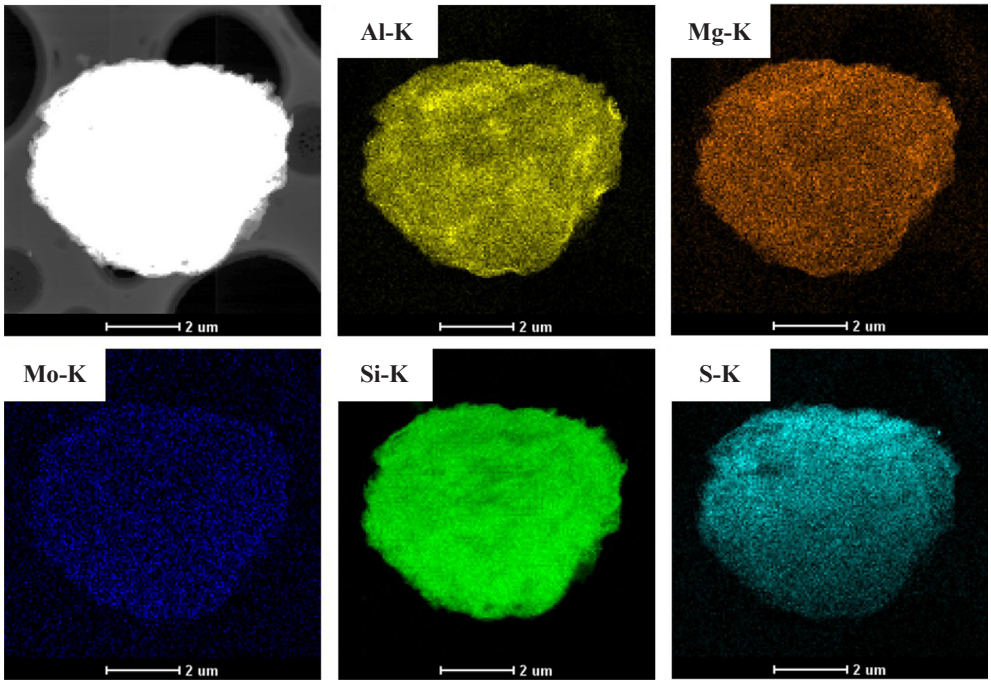

Fig. 3. HAADF-STEM image and the corresponding STEM-EDX elemental mapping images of the SMt/MoS_2 microspheres.

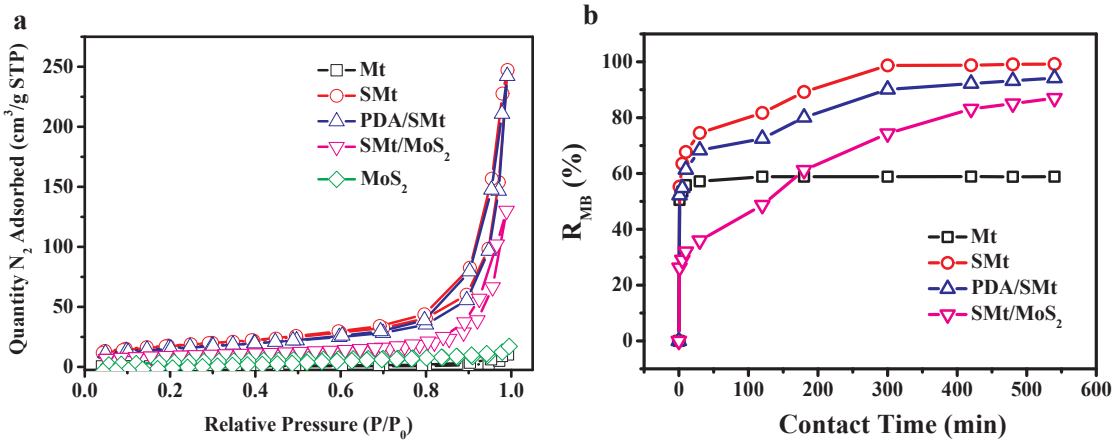

Fig. 4. The N_2 adsorption (a) and adsorption kinetics of model organic pollutant MB (b) on the Mt, SMt, PDA/SMt, and SMt/MoS_2 microspheres.

Table 1
Mesoscale properties of Mt, SMt, PDA/SMt, SMt@MoS_2, and MoS_2.

Sample	BET surface area (m^2 g^{-1})	Pore volume (cm^3 g^{-1})
Mt	8.2	0.10
SMt	60.6	0.38
PDA/SMt	45.6	0.24
SMt@MoS_2	31.3	0.20
MoS_2	16.0	0.03

problems of aggregation and recyclability through self-sedimentary micro-sized porous granular nanomaterials as the substrate may pave a promising way to produce high-performance catalyst for application.

Author contributions

All authors have given approval to the final version of the manuscript.

CRediT authorship contribution statement

Hongzhen Wang: Writing - original draft. **Ning Wang:** Writing -

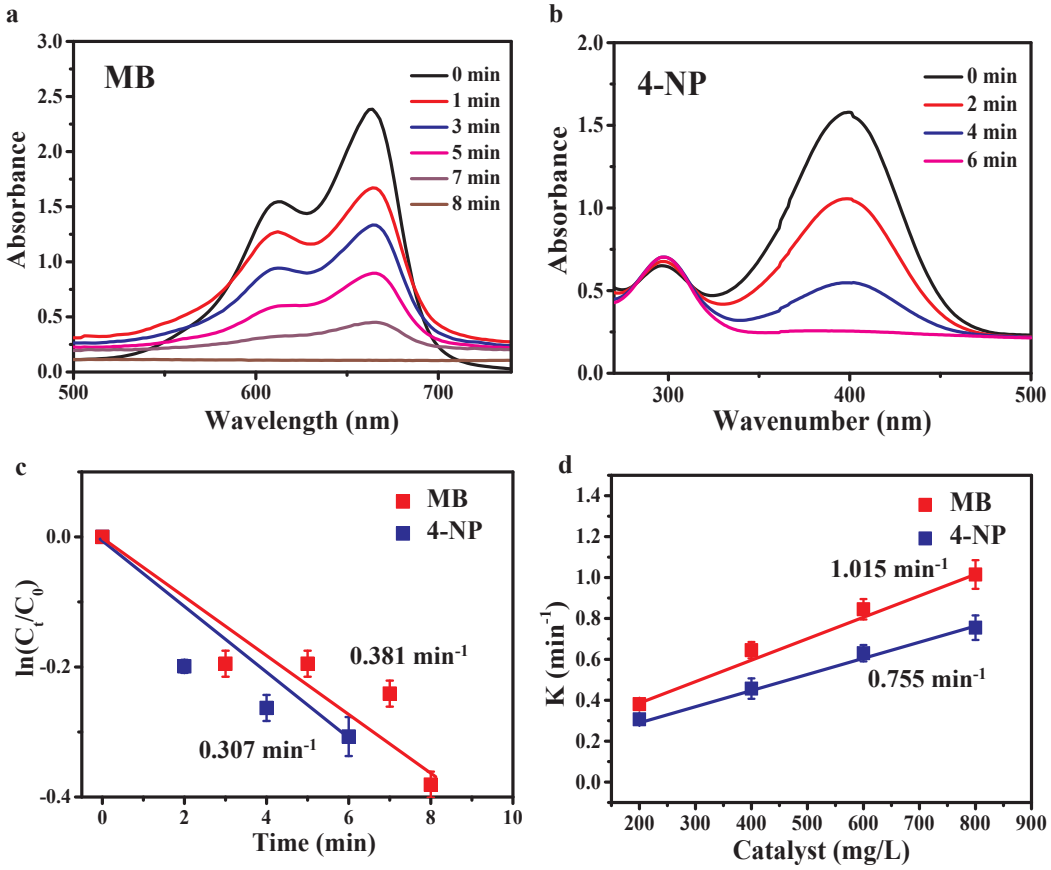

Fig. 5. Time-resolved UV–Vis spectra of MB (a) and 4-NP (b) solutions. Plot of ln (C_t/C_0) versus reaction time for the catalytic reduction of MB and 4-NP (c). The apparent reduction rate constant (K) of MB and 4-NP varies as a function of the concentration of microspheres (d).

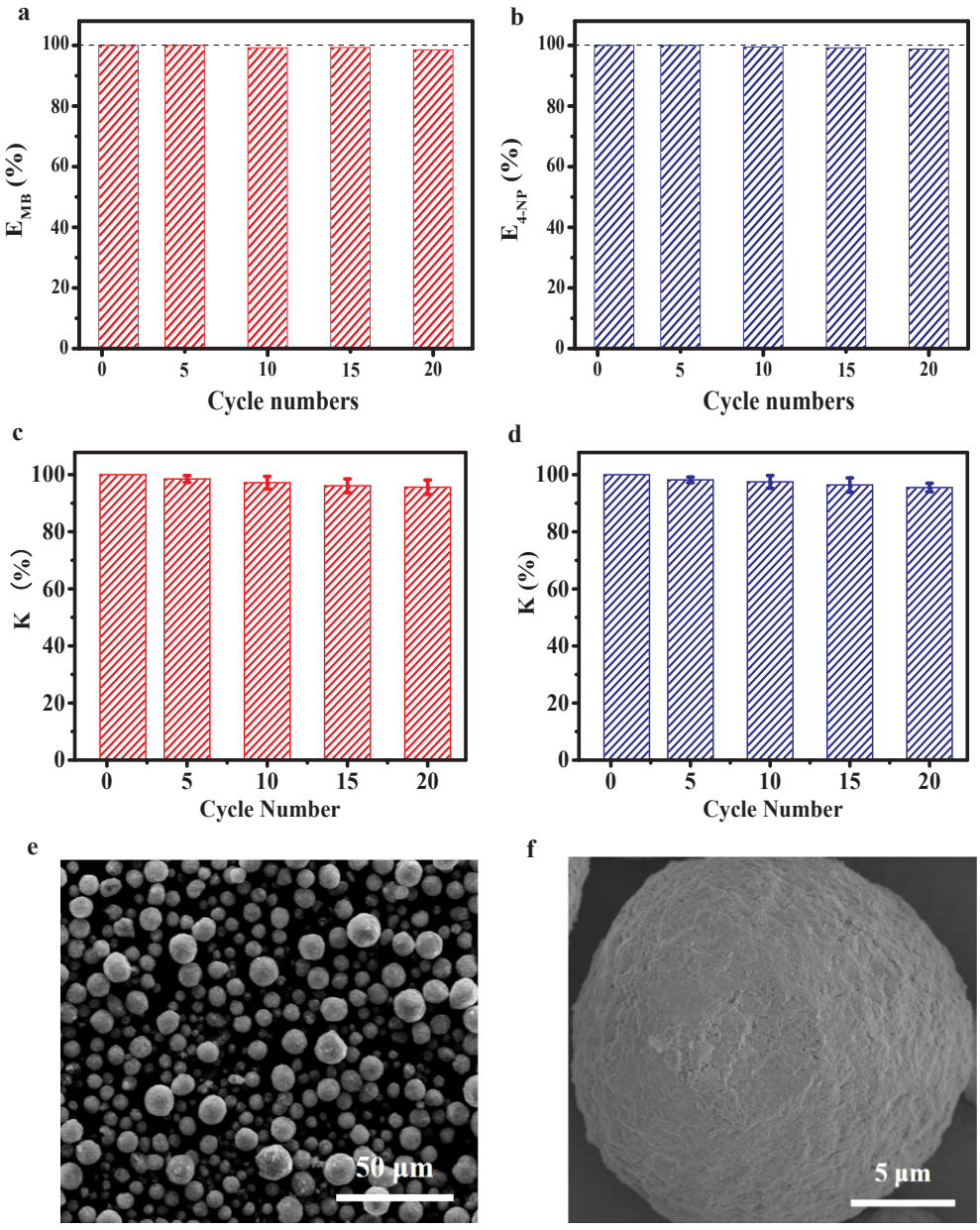

Fig. 6. The changes of apparent reduction rate constants K of microspheres in the reduction of MB (a) and 4-NP (b) with the prolonged cycle number. SEM images of SMt/MoS_2 microspheres after 20 cycles for MB (c) and 4-NP (d), respectively.

review & editing. **Fushuai Wang:** Writing - original draft. **Fengyan Xiao:** Writing - original draft. **Dawei Pan:** Writing - review & editing.

Declaration of Competing Interest

The authors declare that they have no known competing financial interests or personal relationships that could have appeared to influence the work reported in this paper.

Acknowledgments

The authors gratefully acknowledge the funding support from National Natural Science Foundation of China (No. 51703110 and 51903247), Key Science and Technology Program of Yantai City, China (No. 2018ZHGY075) and Shandong Key Laboratory of Coastal Environmental Processes, YICCAS (Grant No. 2019SDHADKFJJ15).

Appendix A. Supplementary material

Supplementary data to this article can be found online at https://doi.org/10.1016/j.seppur.2020.117346.

References

[1] I. Ali, New generation adsorbents for water treatment, Chem. Rev. 112 (2012) 5073–5091.
[2] M. Bordbar, N. Negahdar, M. Nasrollahzadeh, Melissa Officinalis L. leaf extract assisted green synthesis of CuO/ZnO nanocomposite for the reduction of 4-nitrophenol and Rhodamine B, Sep. Purif. Technol. 191 (2018) 295–300.
[3] Y. Wang, G.E. Chen, H.L. Wu, Z.L. Xu, J.J. Wan, L.J. Liu, S.J. Xu, Y.F. Kong, Q. Wu, J. Min, H.F. Mao, Fabrication of GO-Ag/PVDF/F127 modified membrane IPA coagulation bath for catalytic reduction of 4-nitrophenol, Sep. Purif. Technol. 235 (2020) 116143.
[4] Y.X. Wang, S. Ma, M.N. Huang, H. Yang, Z.L. Xu, Z. Xu, Ag NPs coated PVDF@TiO_2 nanofiber membrane prepared by epitaxial growth on TiO_2 inter-layer for 4-NP reduction application, Sep. Purif. Technol. 227 (2019) 115700.
[5] M. Zubair, M. Daud, G. McKay, F. Shehzad, M.A. Al-Harthi, Recent progress in layered double hydroxides (LDH)-containing hybrids as adsorbents for water

remediation, Appl. Clay Sci. 143 (2017) 279–292.
[6] V. Vimonses, S. Lei, B. Jin, C.W.K. Chow, C. Saint, Adsorption of congo red by three Australian kaolins, Appl. Clay Sci. 43 (2009) 465–472.
[7] C.S. Patil, A.N. Kadam, D.B. Gunjal, V.M. Naik, S.W. Lee, G.B. Kolekar, A.H. Gore, Sugarcane molasses derived carbon sheet@sea sand composite for direct removal of methylene blue from textile wastewater: Industrial wastewater remediation through sustainable, greener, and scalable methodology, Sep. Purif. Technol. 247 (2020) 116997.
[8] P. Cartagena, M.E. Kaddouri, V. Cases, A. Trapote, D. Prats, Reduction of emerging micropollutants, organic matter, nutrients and salinity from real wastewater by combined MBR–NF/RO treatment, Sep. Purif. Technol. 110 (2013) 132–143.
[9] W. Zhang, X. Wang, Y. Zhang, B. van Bochove, E. Mäkilä, J. Seppälä, W. Xu, S. Willför, C. Xu, Robust shape-retaining nanocellulose-based aerogels decorated with silver nanoparticles for fast continuous catalytic discoloration of organic dyes, Sep. Purif. Technol. 242 (2020) 116523.
[10] A. Hatamifard, M. Nasrollahzadeh, J. Lipkowski, Green synthesis of a natrolite zeolite/palladium nanocomposite and its application as a reusable catalyst for the reduction of organic dyes in a very short time, RSC Adv. 5 (2015) 91372–91381.
[11] M. Atarod, M. Nasrollahzadeh, S.M. Sajadi, Green synthesis of a Cu/reduced graphene oxide/Fe_3O_4 nanocomposite using Euphorbia wallichii leaf extract and its application as a recyclable and heterogeneous catalyst for the reduction of 4-nitrophenol and rhodamine B, RSC Adv. 5 (2015) 91532–91543.
[12] M. Nasrollahzadeh, M. Sajjadi, M.R. Tahsili, High efficiency treatment of organic/inorganic pollutants using recyclable magnetic N-heterocyclic copper(II) complex and its antimicrobial applications, Sep. Purif. Technol. 238 (2020) 116403.
[13] M. Sajjadi, N.Y. Baran, T. Baran, M. Nasrollahzadeh, M.R. Tahsili, M. Shokouhimehr, Palladium nanoparticles stabilized on a novel Schiff base modified Unye bentonite: Highly stable, reusable and efficient nanocatalyst for treating wastewater contaminants and inactivating pathogenic microbes, Sep. Purif. Technol. 237 (2020) 116383.
[14] S.-M.-G. Yek, D. Azarifar, M. Nasrollahzadeh, M. Bagherzadeh, M. Shokouhimehr, Heterogenized Cu(II) complex of 5-aminotetrazole immobilized on graphene oxide nanosheets as an efficient catalyst for treating environmental contaminants, Sep. Purif. Technol. 247 (2020) 116952.
[15] Z. Zhang, D. Jiang, D. Li, M. He, M. Chen, Construction of $SnNb_2O_6$ nanosheet/g-C_3N_4 nanosheet two-dimensional heterostructures with improved photocatalytic activity: Synergistic effect and mechanism insight, Appl. Catal., B 183 (2016) 113–123.
[16] H. Zhang, Ultrathin two-dimensional nanomaterials, ACS Nano 9 (2015) 9451–9469.
[17] S. Kumar, V. Sharma, K. Bhattacharyya, V. Krishnan, N-doped ZnO-MoS_2 binary heterojunctions: the dual role of 2D MoS_2 in the enhancement of photostability and photocatalytic activity under visible light irradiation for tetracycline degradation, Mater. Chem. Front. 1 (2017) 1093–1106.
[18] L. Guardia, J.I. Paredes, J.M. Munuera, S. Villar-Rodil, J.M.D. Tascon, Chemically exfoliated MoS_2 nanosheets as an efficient catalyst for reduction reactions in the aqueous phase, ACS Appl. Mater. Inter. 6 (2014) 21702–21710.
[19] V.O. Koroteev, L.G. Bulusheva, I.P. Asanov, E.V. Shlyakhova, D.V. Vyalikh, A.V. Okotrub, Charge transfer in the MoS_2/carbon nanotube composite, J. Phys. Chem. C 115 (2011) 21199–21204.
[20] S. Chakrabarty, A. Mukherjee, S. Basu, RGO-MoS_2 supported $NiCo_2O_4$ catalyst toward solar water splitting and dye degradation, ACS Sustain. Chem. Eng. 6 (2018) 5238–5247.
[21] N. Meng, J. Cheng, Y. Zhou, W. Nie, P. Chen, Green synthesis of layered 1T-MoS_2/reduced graphene oxide nanocomposite with excellent catalytic performances for 4-nitrophenol reduction, Appl. Surf. Sci. 396 (2017) 310–318.
[22] A. Pal, T.K. Jana, T. Roy, A. Pradhan, K. Chatterjee, MoS_2-TiO_2 nanocomposite with excellent adsorption performance and high antibacterial activity, Chemistryselect 3 (2018) 81–90.
[23] P. Chen, S. Zeng, Y. Zhao, S. Kang, T. Zhang, S. Song, Synthesis of unique-morphological hollow microspheres of MoS_2@montmorillonite nanosheets for the enhancement of photocatalytic activity and cycle stability, J. Mater. Sci. Technol. 41 (2020) 88–97.
[24] W. Wang, T. Wen, H. Bai, Y. Zhao, J. Ni, L. Yang, L. Xia, S. Song, Adsorption toward Cu(II) and inhibitory effect on bacterial growth occurring on molybdenum disulfide-montmorillonite hydrogel surface, Chemosphere 248 (2020) 126025.
[25] L. Yang, Q. Wang, J.R. Rangel-Mendez, F. Jia, S. Song, B. Yang, Self-assembly montmorillonite nanosheets supported hierarchical MoS_2 as enhanced catalyst toward methyl orange degradation, Mater. Chem. Phys. 246 (2020) 122829.
[26] E.D.A. Mário, C. Liu, C.I. Ezugwu, S. Mao, F. Jia, S. Song, Molybdenum disulfide/montmorillonite composite as a highly efficient adsorbent for mercury removal from wastewater, Appl. Clay Sci. 184 (2020) 105370.
[27] K. Peng, H. Wang, H. Gao, P. Wan, M. Ma, X. Li, Emerging hierarchical ternary 2D nanocomposites constructed from montmorillonite, graphene and MoS_2 for enhanced electrochemical hydrogen evolution, Chem. Eng. J. 124704 (2020).
[28] A. Joseph, K. Vellayan, B. González, M.A. Vicente, A. Gil, Effective degradation of methylene blue in aqueous solution using Pd-supported Cu-doped Ti-pillared montmorillonite catalyst, Appl. Clay Sci. 168 (2019) 7–10.
[29] Q. Zhang, Z. Yan, J. Ouyang, Y. Zhang, H. Yang, D. Chen, Chemically modified kaolinite nanolayers for the removal of organic pollutants, Appl. Clay Sci. 157 (2018) 283–290.
[30] K. Peng, L. Fu, H. Yang, J. Ouyang, A. Tang, Hierarchical MoS2 intercalated clay hybrid nanosheets with enhanced catalytic activity, NANO Res. 10 (2017) 570–583.
[31] K. Peng, J. Wang, H. Wang, X. Li, P. Wan, H. Zhang, L. Bai, MoS2 nanosheets supported on carbon hybridized montmorillonite as an efficient heterogeneous catalyst in aqueous phase, Appl. Clay Sci. 183 (2019) 105346.
[32] A. Stunda-Zujeva, Z. Irbe, L. Berzina-Cimdina, Controlling the morphology of ceramic and composite powders obtained via spray drying-A review, Ceram. Int. 43 (2017) 11543–11551.
[33] Y. Qin, N. Wang, Y. Zhou, Y. Huang, H. Niu, J.Y. Dong, Fabrication of nanofillers into a granular “Nanosupport” for Ziegler-Natta catalysts: Towards scalable in situ preparation of polyolefin nanocomposites, Macromol. Rapid Commun. 32 (2011) 1052–1059.
[34] N. Wang, F. Xiao, J. Zhang, H. Zhou, Y. Qin, D. Pan, Spherical montmorillonite-supported nano-silver as a self-sedimentary catalyst for methylene blue removal, Appl. Clay Sci. 174 (2019) 146–151.
[35] F. Xiao, H. Ren, H. Zhou, H. Wang, N. Wang, D. Pan, Porous montmorillonite@graphene oxide@Au nanoparticle composite microspheres for organic dye degradation, ACS Appl. Nano Mater. 2 (2019) 5420–5429.
[36] F. Xiao, Y. Qin, N. Wang, D. Pan, Towards mass production of Au nanoparticles supported on montmorillonite microspheres for catalytic reduction of 4-nitrophenol, Appl. Clay Sci. 166 (2018) 74–79.
[37] N. Wang, Z. Zhang, J. Huang, Y. Hu, Facile synthesis of copper ions chelated sand via dopamine chemistry for recyclable and sustainable catalysis, Chem. Eng. Sci. 203 (2019) 312–320.
[38] Y. Liu, K. Ai, L. Lu, Polydopamine and its derivative materials: synthesis and promising applications in energy, environmental, and biomedical fields, Chem. Rev. 114 (2014) 5057–5115.
[39] N. Wang, Y. Hu, Z. Zhang, Sustainable catalytic properties of silver nanoparticles supported montmorillonite for highly efficient recyclable reduction of methylene blue, Appl. Clay Sci. 150 (2017) 47–55.
[40] W.P. Gonçalves, V.J. Silva, R.R. Menezes, G.A. Neves, H.L. Lira, L.N.L. Santana, Microstructural, physical and mechanical behavior of pastes containing clays and alumina waste, Appl. Clay Sci. 137 (2017) 259–265.
[41] Y. Tan, K. Yu, T. Yang, Q. Zhang, W. Cong, H. Yin, Z. Zhang, Y. Chen, Z. Zhu, The combinations of hollow MoS2 micro@nano-spheres: one-step synthesis, excellent photocatalytic and humidity sensing properties, J. Mater. Chem. C 2 (2014) 5422–5430.